Advances in Nanochemistry

Article

Facile synthesis of nanoporous spinel nickel-manganese-cobalt ternary oxide hollow spheres as high-performance supercapacitor electrode material

Received 2nd January 2020,
Accepted 7th January 2020,
DOI:10.22126/anc.2020.4909.1021

Seyyed Ebrahim Moosavifard *[,1,2], Foroogh Najafi [1], Mohammad Izadi [1], Zahra Gharibzadeh [1], Zahra Habibi [1]

[1] Department of Advanced Medical Sciences & Technologies, School of Medicine, Jahrom University of Medical Sciences, Jahrom, Iran.
[2] Research Center for Noncommunicable Diseases, School of Medicine, Jahrom University of Medical Sciences, Jahrom, Iran.

Abstract

Design and synthesis of new and high-performance electrode materials are the tasks of scientists to respond to the increasing demand for efficient renewable energy storage devices. Herein, we developed a spinel nickel-manganese-cobalt ternary oxide (NMCO) spheres by a facile approach with a hollow-interior nanoporous shell possessing a high specific surface area of 67 $m^2 g^{-1}$ and pore size distribution of about 8 nm as a high-performance electrode material for supercapacitor applications. This electrode delivers ultrahigh specific capacitance of 1372 F g^{-1} at 2 A g^{-1} (4.1 F cm^{-2} at 6 mA cm^{-2}) with remarkable rate capability of 55% after increasing the current density from 2 A g^{-1} (6 mA cm^{-2}) to 60 A g^{-1} (180 mA cm^{-2}), excellent cycling stability of 91.2% after 10000 continues charge/discharge cycles at 15 mA cm^{-2}, and maximum energy density of 38.6 Wh kg^{-1}. This work sheds further light on the design and development of high-performance electrode materials not only for energy storage applications but also for other electronic devices.

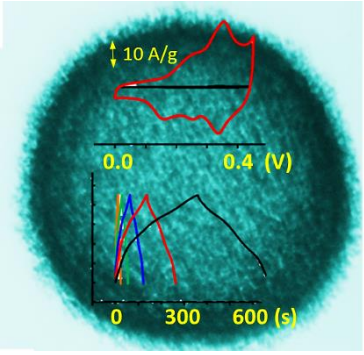

Keywords: *Nanoporous, Spinel, Ternary oxide, Hollow spheres, Supercapacitor.*

Introduction

In the twenty-first century, the development of clean and renewable energy sources has been one of the most important tasks of scientists due to increasing energy consumption, global warming challenges, and rapid depletion of fossil fuels.[1-3] Fuel cells, lithium-ion batteries, and supercapacitors (SCs) are promising renewable electrochemical energy storage systems. Due to greater energy density than conventional capacitors, higher power density, and cyclability than batteries, SCs have attracted more and more attention.[4] But, the application of supercapacitors has been limited owing to their lower energy density than rechargeable batteries.[5] Besides extraordinary power density, long cycle life, and fast charge/discharge rates the advanced supercapacitors benefit from low-cost electrode materials with a unique morphology.[6,7] In this point of view, carbonaceous materials have been extensively employed. However, in practice, the electrochemical properties of carbonaceous materials are mainly limited by their strong aggregation and severely active surface area reduction. Furthermore, their low energy density is still a challenge due to the electrical double layer capacitance (EDLC) mechanism that stores charge at the electrode/electrolyte interface.[8]

On the other hand, transition metal oxides such as NiO,[9] Co_3O_4,[10] $NiCo_2O_4$,[11] $CuCo_2O_4$,[12] MnO_2,[13] and CuO[14] can provide higher specific capacitance and energy density than EDLCs due to their pseudocapacitance mechanism which store energy by fast and reversible Faradaic redox reactions at the electrode/electrolyte interface.[15] Among the various transition metals, nickel, manganese, and cobalt have attracted great interest because of high electrochemical activity, low cost, and abundant oxide/hydroxide compounds.[1,16] On the other hand, it is demonstrated that the mixed metal oxides such as binary or ternary of them deliver much better electrochemical performance due to richer electron valence and synergistic effects between the metal ions.[17]

Another critical factor strongly affects the electrochemical performance of the electrode materials is their morphology.[18] The morphologies that can provide porous structures with the high specific surface area are more efficient. Among different morphologies, hollow spheres have attracted much consideration due to short distances for mass/charge transfer and high weight fraction of active species.[19]

Heydari et. al. synthesized CuS nano-hollow spheres via a polyol rout with a maximum specific capacitance of 948 F g^{-1} and 9.2% loss after the 2000 cycles.[20] Mohammadi et. al. prepared $CuCo_2S_4$ microspheres by a self-template method as a novel positive

Corresponding author:
Seyyed Ebrahim Moosavifard, Email: info_seyyed@yahoo.com

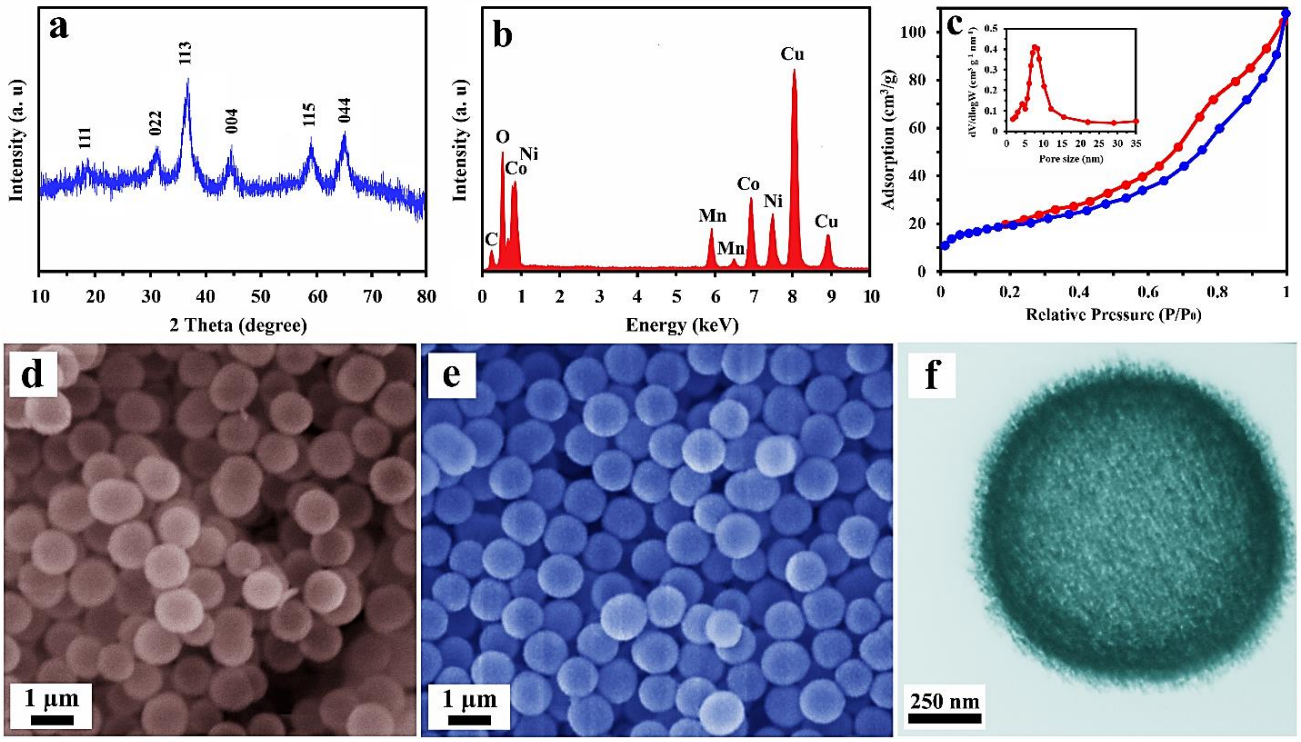

Figure 1. *(a) XRD pattern of the NMCO sample, (b) EDAX spectrum of the NMCO sample, (c) nitrogen adsorption/desorption isotherms of the sample (inset is the BJH pore size distribution), (d) typical SEM image of the NiMnCo-glycerate particles, (e) typical SEM image of the NMCO microspheres, and (f) typical TEM image of a NMCO hollow microsphere.*

electrode for hybrid energy storage devices with a specific capacitance of 1566 F g^{-1} and 95.7% retention after 5000 cycles.[17] Ensafi et. al. developed onion-like $CuCo_2O_4$ hollow spheres derived from bimetal-organic frameworks with a maximum specific capacitance of 1700 F g^{-1}.[21] Saleki et. al. reported a metal-organic framework (MOF) assistance synthesis of double-shelled $CuCo_2O_4$ hollow spheres with a specific capacity of 701 C g^{-1} and 6.4% loss after the 6000 cycles.[19]

In this work, for the first time, we develop a nanoporous nickel-manganese-cobalt ternary oxide (NMCO) hollow spheres synthesized via a glycerate procedure as a high-performance supercapacitor electrode material. This NMCO electrode delivers an ultrahigh specific capacitance of 1310 F g^{-1} at 2 A g^{-1} with excellent rate capability and outstanding cycling stability, demonstrating its potential as a high-performance electrode material for supercapacitor applications.

Experimental

Synthesis of nanoporous NMCO hollow spheres

All chemicals used in this work are of analytical grade and applied without additional purification. In a typical procedure for the synthesis of NMCO hollow spheres, 72.5 mg of $Co(NO_3)_2{\cdot}6H_2O$, 62.7 mg of $Mn(NO_3)_2{\cdot}4H_2O$ and 72.5 mg of $Ni(NO_3)_2{\cdot}6H_2O$ were added to a stirred solution of 10 mL of glycerol and 50 mL isopropanol to achieve a homogeneous apparent solution. The resulting solution was transferred into a Teflon-lined stainless-steel autoclave and maintained at 180 ˚C for 6 h. After cooling down to room temperature, the as-prepared NiMnCo-glycerate precursors were separated and dried at 80 ˚C. The hollow NMCO spheres were also synthesized by annealing of NiMnCo-glycerate precursors at 400 ˚C in air for 2 h with a heating rate of 1 ˚C min^{-1}.

Characterization

Structural characterization was done by an X-ray powder diffraction (XRD, Philips X'pert diffractometer with Co Kα radiation). Nitrogen adsorption/desorption, specific surface area and pore size distributions were performed by a Micromeritics ASAP-2010 apparatus at 77 K. The morphologies and structural investigations were investigated using a Zeiss scanning electron microscope (SEM) and a Philips EM 208 transmission electron microscope (TEM). Electrochemical measurements were performed on a WonATech Zive SP1 device.

Electrochemical measurements

An aqueous 3 M KOH solution was used as the electrolyte in all electrochemical measurements. The electrode was prepared by mixing the active material, acetylene black, and polyvinylidene fluoride in N-methyl-2-pyrrolidone (PVDF in NMP) with a mass ratio of 85:10:5. The mixture was coated by a spatula on a piece of nickel foam as the current collector and then dried in 120 ◦C for 2 h. The mass loading on the electrodes was about 3 mg cm^{-2}. The as-prepared electrode was applied as the working electrode, while an Hg/HgO electrode and a platinum plate were used as the reference and counter electrodes, respectively.

The specific capacitances (C_{sp}), energy densities (ED, Wh kg^{-1}), and power densities (PD, W kg^{-1}) were calculated from the discharge curves using the following equations:

$$C_{sp} = \frac{I\Delta t}{m\Delta V} \quad (1)$$

$$ED = \frac{C_{sp}\Delta V^2}{2} \quad (2)$$

$$PD = \frac{ED}{\Delta t} \quad (3)$$

Where I is the discharge current (A), Δt is the discharge time (s), ΔV is the potential window (V), and m is the mass loading (g).

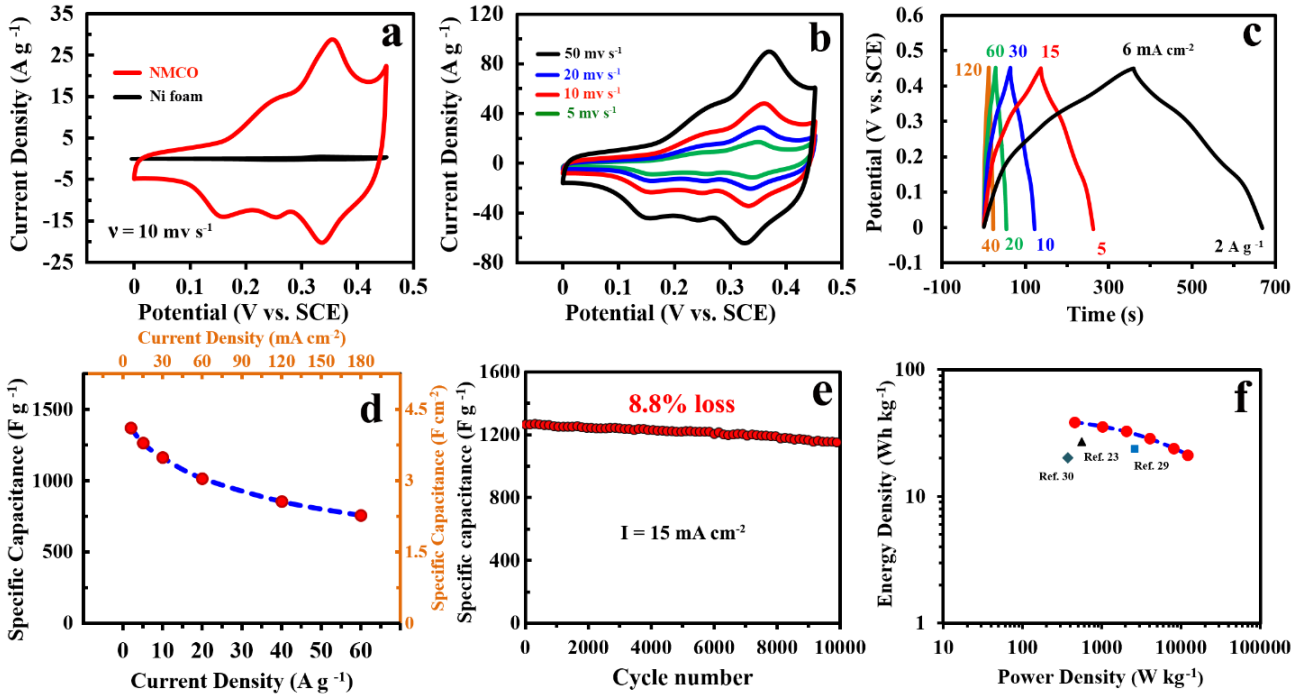

Figure 2. *(a) CV curves of the NMCO electrode and Ni substrate at a scan rate of 10 mV s^{-1}, (b) CV curves of the NMCO electrode at various scan rates, (c) CD curves of the NMCO electrode at different current densities, (d) rate capability of the electrode at different gravimetric and areal current densities, (e) cycling stability of the electrode during 10000 continues CD cycles at a current density of 15 mA cm^{-2}, and (f) Ragone plot of the electrode.*

Results and discussion

The crystalline structure of the as-prepared sample was explored by XRD analysis as shown in Figure 1a. All diffraction peaks can be well indexed to the standard pattern of the cubic spinel phase (JCPDS 98-009-8472) with the space group *Fd-3m*.[22,23] The broad diffraction peaks verify the existence of small size crystallites. Figure 1b presenting the EDAX result of the NMCO sample further demonstrate the purity of the mixed transition metal oxide. Nitrogen adsorption/desorption isotherms were also recorded to determine the porosity of the as-prepared hollow spheres. As can be seen in Figure 1c, NMCO hollow spheres sample delivered an isotherm with a hysteresis loop that is characteristic for nanoporous materials.[24] Furthermore, the BET specific surface area of 67 m^2 g^{-1} was calculated for it. The BJH analysis (inset of Figure 1c) further confirms the nanoporous structure of the sample with narrow pore size distribution centered at about 8 nm.

The morphology of the NiMnCo-glycerate precursors and NMCO hollow spheres samples were investigated by scanning electron microscopy (SEM). As shown in Figure 1d, NiMnCo-glycerate particles have a spherical morphology with a uniform size of about 1 µm. Figure 1e shows the SEM image of the sample after calcination at 400 ˚C in air for 2 h. Obviously, the NMCO particles have well preserved their spherical morphology after the heat treatment process. In order to investigate the interior structure of the NMCO microspheres, transmission electron microscopy (TEM) was used. Figure 1f displays the TEM image of an NMCO microsphere. As can be seen, the microsphere has a hollow interior with the nanoporous shell which is in good agreement with the result of BET and SEM analyses.

Electrochemical evaluation

The electrochemical measurements were done in a three-electrode system containing 3 mol L^{-1} KOH as the electrolyte. The comparative cyclic voltammetry (CV) curves of the NMCO electrode and the Ni foam at a sweep rate of 10 mV s^{-1} are depicted in Figure 2a. It is obvious that the NMCO electrode possesses a very large surrounded area illustrating its significant charge storage. In addition, the straight line derived from Ni foam confirms that the capacitance contribution of the substrate is insignificant. Figure 2b presents the typical CV curves at various sweep rates (5 to 50 mV s^{-1}) for the NMCO electrode. CV curves consist of some well-defined redox peaks, attributing to the reversible Faradaic reaction processes of transition metal ions that reveal the pseudo-capacitive characteristics of the electrode.[18, 22] Meanwhile, with the increase of sweep rate, the shape of CV curves remains approximately unchanged suggesting the excellent rate capability and fast redox reactions at the interface of electrode/electrolyte.[25,26] Figure 2c represents the charge/discharge (CD) curves of the NMCO electrode at different current densities in a potential window of 0 to 0.45 V. The shape of the curves with the voltage plateaus well agrees with the CV curves and verifies the reversible Faradaic reactions at the surface of the electrode.[27] The specific capacitance values for the NMCO electrode, according to the discharge time, are illustrated in Figure 2d. The NMCO electrode exhibited an ultrahigh gravimetric capacitance of 1372 F g^{-1} at 2 A g^{-1} (4.1 F cm^{-2} at 6 mA cm^{-2}). These values are much more than the values reported previously.[8,10,14,23-25,28] Also, this electrode maintained 55% of its initial capacitance after increasing the current density from 2 A g^{-1} (6 mA cm^{-2}) to 60 A g^{-1} (180 mA cm^{-2}), which demonstrates the superior rate capability of the electrode. The cycling stability of the electrode was also investigated during 10000 CD cycles at a current density of 5 A g^{-1} (15 mA cm^{-2}) as shown in Figure 2e. The excellent

cycling stability of the electrode was confirmed by only 8.8% loss in its capacitance after 10000 continues CD cycles. Energy and power density are other parameters that investigated for evaluating the overall performance of the electrode. As shown in Figure 2f, the NMCO electrode delivered a maximum energy density of 38.6 Wh kg^{-1} with a maximum power density of 12.15 kW kg^{-1}. These values are much more than the values reported previously for ternary NiMnCo electrodes.[23,29,30]

The excellent electrochemical performance of the electrode including ultrahigh specific capacitance, remarkable rate capability and cycling stability, and high energy and power densities can be related to the type of the electrode material and its unique structure.[31,32] In the former, the ternary metal oxides possess rich valence electrons that enhance electrochemical activity and reduce electrical resistance.[33,34] In the latter, the hollow spheres with nanoporous shells enhance the specific surface area, reduce mass- and electron-transfer distance, and facilitate the accessibility of the electrolyte.[35-37]

Conclusion

In summary, for the first time, a spinel nickel-manganese-cobalt ternary oxide was synthesized in hollow sphere morphology with nanoporous shell and high specific surface area, as a high-performance electrode material for supercapacitor applications. The electrode delivered ultrahigh specific capacitances with outstanding rate capability, high energy density, and remarkable cycling stability at different current densities. The excellent electrochemical performance of the electrode was attributed to the type of the electrode material and its unique structure. This work not only introduces new high-performance electrode material for supercapacitor applications but also gives some insights into the development of mixed transition metal oxides electrodes for various range of applications such as lithium-ion batteries, catalysis, and other electronic devices.

References

1. L. Zhang, D. Shi, T. Liu, M. Jaroniec, and J. Yu, *Materials Today*, 25, **2019**, 35.
2. J. S. Chae, S. K. Park, K. C. Roh, and H. S. Park, *Energy Storage Mater.*, 24, **2020**, 113.
3. A. Berrueta, A. Ursúa, I. S. Martín, A. Eftekhari, and P. Sanchis, *IEEE Access*, 7, **2019**, 50869.
4. A. Muzaffar, M. B. Ahamed, K. Deshmukh, and J. Thirumalai, *Renew. Sust. Energ. Rev.*, 101, **2019**, 123.
5. S. E. Moosavifard, J. Shamsi, and M. Ayazpour, *Ceram. Int.*, 41, **2015**, 1831.
6. X.-C. Xie, K.-J. Huang, and X. Wu, *J. Mater. Chem. A*, 6, **2018**, 6754.
7. K.-C. Ho and L.-Y. Lin, *J. Mater. Chem. A*, 7, **2019**, 3516.
8. K. Xu, S. Ma, Y. Shen, Q. Ren, J. Yang, X. Chen, and J. Hu, *Chem. Eng. J.*, 369, **2019**, 363.
9. S. Liu, S. C. Lee, U. M. Patil, C. Ray, K. V. Sankar, K. Zhang, A. Kundu, S. kang, J. H. Park, and S. Chan Jun, *J. Mater. Chem. A*, 5, **2017**, 4543.
10. W. Wang, Y. Yuan, J. Yang, L. Meng, H. Tang, Y. Zeng, Z. Ye, and J. Lu, *J. Mater. Sci.*, 53, **2018**, 6116.
11. C. Wei, X. Zheng, R. Li, X. Wang, Z. Xaio, and L. Wang, *ChemistrySelect*, 4, **2019**, 11149.
12. A. Pendashteh, S. E. Moosavifard, M. S. Rahmanifar, Y. Wang, M. F. El-Kady, R. B. Kaner, and M. F. Mousavi, *Chem. Mater.*, 27, **2015**, 3919.
13. S. Zhu, L. Li, J. Liu, H. Wang, T. Wang, Y. Zhang, L. Zhang, R. S. Ruoff, and F. Dong, *ACS Nano*, 12, **2018**, 1033.
14. S. E. Moosavifard, J. Shamsi, S. Fani, and S. Kadkhodazade, *Ceram. Int.*, 40, **2014**, 15973.
15. W. Jin and G. Maduraiveeran, *Mater. Today Energy*, 13, **2019**, 64.
16. P. Zhang, F. Wang, M. Yu, X. Zhuang, and X. Feng, *Chem. Soc. Rev.*, 47, **2018**, 7426.
17. A. Mohammadi, S. E. Moosavifard, A. Goljanian Tabrizi, M. M. Abdi, and G. Karimi, *ACS Appl. Mater. Interfaces*, 2, **2018**, 627.
18. S. E. Moosavifard, S. K. Kaverlavani, J. Shamsi, and A. Bakouei, *J. Mater. Chem. A*, 5, **2017**, 18429.
19. F. Saleki, A. Mohammadi, S. E. Moosavifard, A. Hafizi, and M. R. Rahimpour, *J. Colloid Interface Sci.*, 556, **2019**, 83.
20. H. Heydari, S. E. Moosavifard, S. Elyasi, and M. Shahraki, *Appl. Surf. Sci.*, 394, **2017**, 425.
21. A. A. Ensafi, S. E. Moosavifard, B. Rezaei, and S. K. Kaverlavani, *J. Mater. Chem. A*, 6, **2018**, 10497.
22. A. Pendashteh, J. Palma, M. Anderson, and R. Marcilla, *Appl. Catal. B*, 201, **2017**, 241.
23. J. S. Sanchez, A. Pendashteh, J. Palma, M. Anderson, and R. Marcilla, *Electrochim. Acta*, 279, **2018**, 44.
24. A. Namdarian, A. G. Tabrizi, A. Maseleno, A. Mohammadi, and S. E. Moosavifard, *Int. J. Hydrogen Energy*, 43, **2018**, 17780.
25. S. E. Moosavifard, M. F. El-Kady, M. S. Rahmanifar, R. B. Kaner, and M. F. Mousavi, *ACS Appl. Mater. Interfaces*, 7, **2015**, 4851.
26. S. E. Moosavifard, S. Fani, and M. Rahmanian, *Chem. commun.*, 52, **2016**, 4517.
27. S. E. Moosavifard, J. Shamsi, M. K. Altafi, and Z. S. Moosavifard, *Chem. commun.*, 52, **2016**, 13140.
28. H. Heydari, S. E. Moosavifard, M. Shahraki, and S. Elyasi, *J. Energy Chem.*, 26, **2017**, 762.
29. A. Reghu Nath, A. Jayachandran, and N. Sandhyarani, *Dalton Trans.*, 48, **2019**, 4211.
30. A. Pendashteh, J. Palma, M. Anderson, and R. Marcilla, *RSC Adv.*, 6, **2016**, 28970.
31. S. Kamari Kaverlavani, S. E. Moosavifard, and A. Bakouei, *Chem. commun.*, 53, **2017**, 1052.
32. S. K. Kaverlavani, S. E. Moosavifard, and A. Bakouei, *J. Mater. Chem. A*, 5, **2017**, 14301.
33. F. Ma, X. Dai, J. Jin, N. Tie, and Y. Dai, *Electrochim. Acta*, 331, **2020**, 135459.
34. A. Mohammadi, N. Arsalani, A. G. Tabrizi, S. E. Moosavifard, Z. Naqshbandi, and L. S. Ghadimi, *Chem. Eng. J.*, 334, **2018**, 66.
35. S. E. Moosavifard, J. Shamsi, S. Fani, and S. Kadkhodazade, *RSC Adv.*, 4, **2014**, 52555.
36. H. Ren and R. Yu, *Inorg. Chem. Front.*, 6, **2019**, 2239.
37. C. Su, S. Xu, L. Zhang, X. Chen, G. Guan, N. Hu, Y. Su, Z. Zhou, H. Wei, Z. Yang and Y. Qin, *Electrochim. Acta*, 305, **2019**, 81.